Topology optimisation of gridshell structures using a density-based approach

Yongpeng HE*, [a], Paul SHEPHERD [a], Jie WANG [a]

*, [a] Department of Architecture and Civil Engineering, University of Bath, Bath, UK. BA2 7AY
Email: yh2173@bath.ac.uk

Abstract

Gridshells are one of the best ways to cover a large space without introducing intermediate structural supports. However, their vulnerability in terms of stability and moment resisting capacity can also bring severe challenges when determining an optimal design. In order to increase the structural stability and moment stiffness whilst maintaining efficient material placement, this paper explores the introduction of second-layer grids, not across the entire structure, but only in areas where such additional stiffness is necessary. A density-based topology optimisation method, formulated within the framework of the Solid Isotropic Material with Penalization (SIMP) approach, is adopted to determine the paths along which the second-layer grids should be configured. To demonstrate the feasibility of the SIMP method to discrete structures, several benchmark examples are analysed. Under uniformly distributed loads, the relationship between the initial and minimal stiffness of the elements in the SIMP formulation is found to be a key factor in achieving binary topology optimisation results as to whether or not there should be elements present at any given location. The mechanical analysis of the structures shows that the obtained partial double-layer gridshell is more stable and material-saving compared to the single-layer gridshell under the specified load.

Keywords: Topology optimisation, gridshell structure, SIMP approach, uniformly distributed load.

1. Introduction

Gridshell structures are generally accepted to be amongst the most efficient designs to cover large column-free spaces. They take advantage of double-curvature to provide geometrical stiffness out of plane and transfer the applied loads mainly through axial force to the boundary. Large compression forces may appear, especially near the boundary or along the main in-plane load paths. In this way, a loss of stability at some part of the structure, or even globally, may occur, and can result in severe damage. Additionally, gridshell structures could be vulnerable in terms of their moment resisting capacity, since their structural depth is comparatively low compared to the span. In order to increase the flexural stiffness and structural stability, a second-layer of grid is often introduced, which can significantly increase the effective structural depth. In this paper, the authors explore the introduction of secondary layers of structure in specific areas of the gridshell. By configuring second-layer grids only where necessary can effectively enhance the gridshell and bring extra economic benefits.

However, the identification of rational paths for configuration of second-layer grids remains a challenging problem. Extra difficulties may arise when free-form gridshells are considered, since they can have complex geometries, radically varying curvatures, randomly distributed internal openings and irregularly boundary conditions. Similar issues have been investigated when dealing with problems of mesh generation (Su *et al.* [1]), rib/stiffener design for plate and continuous shell structures (Li *et al.* [2], Tam and Muller [3], Michalatos and Kaijima [4], Wang *et al.* [5], Ji *et al.* [6], Lam and Santhikumar [7]). The methods adopted for the research reported in this paper is drawn from the field of continuum

topology optimisation (Sigmund [8], Sigmund [9]), and a SIMP (Solid Isotropic Material with Penalization) approach is implemented. The SIMP approach is applied here to discrete structures modelled with beam elements, rather than continuous structures modelled with continuum elements. This work proposes a method for identifying the paths, along which second-layer grids can be configured. In the following section, the problem formulation and optimisation procedures are introduced. Section 3 presents two benchmark examples and Section 4 discusses the reasons behind the less-than-ideal results. Section 5 then provides two extended examples with enhanced outcomes. Section 6 presents the formation of the partial double-layer gridshell and the mechanical analysis results of the single-layer and partial double-layer gridshells. The conclusions that can be drawn from this investigation are summarized in the final section.

2. Problem formulation and optimisation procedure

2.1. Compliance minimization problem

In order to obtain a practical and rational solution to a topology optimisation problem, it is crucial that the objectives and constraints are properly determined. Stresses and displacements can reflect the strength and stiffness, respectively, but might only be representative of a local part of the structure. Structural compliance, defined as the sum of the loads multiplying with the displacements, is a metric that can reflect the global structural stiffness. The results obtained by minimizing structural compliance are usually taken as the representation of the optimal material distribution under the external load and can be viewed as the force paths. Therefore, minimizing structural compliance is set as the objective function for this work and it is expected that the topology optimisation results can provide rational suggestions on the configuration paths for second-layer grids.

Another consideration is that the obtained topological results should display comparative coarseness. If the resulting paths were densely distributed, the partial double-layer gridshell generated by adding second-layer grids under these paths would be little different compared to a fully double-layer gridshell. On the other hand, if the paths were too coarse, the addition of the second-layer grids might not be sufficient and the resulting partially double-layer gridshell might display little enhanced effect compared to the single-layer solution. Therefore, a constraint function that can control the coarseness of the obtained paths is needed, and it is set as the material volume constraint for this work.

Given the above considerations, the optimisation problems of identifying configuration paths for the addition of second-layer grids, for partially double-layered gridshell structures, can thus be formulated as:

$$\min \quad C(\boldsymbol{X}) = \boldsymbol{U}^T \boldsymbol{K} \boldsymbol{U} = \sum_{e=1}^{n} E_e(x_e) u_e^T k_e u_e$$

$$s.t. \quad \boldsymbol{K} \boldsymbol{U} = \boldsymbol{F}$$

$$V(\boldsymbol{X}) = \sum_{e=1}^{n} x_e A_e l_e \leq \alpha V_0$$

$$x_e \in [0, 1] \tag{1}$$

where x_e is the pseudo physical density of element, with a value of 0 indicating that the element is removed and 1 meaning that the element is maintained, $\boldsymbol{X}$ is the vector of design variables. l_e and A_e are the length and cross-sectional area of element, respectively; α is the user-defined material volume fraction; k_e and u_e the element stiffness and deformation in the local coordinate system, respectively, and $E_e(x_e)$ the material stiffness of the element, hence $E_e(x_e)\, u_e^{\mathrm{T}} k_e u_e$ represents the elemental strain energy.

In topology optimisation of continuum structures, the Solid Isotropic Material with Penalization (SIMP) approach has been widely adopted to facilitate the polarization of design variables (Sigmund [8], Sigmund [9]). Following the modified SIMP approach provided in (Sigmund [9]), the elemental material stiffness can be defined as a function of its pseudo physical density:

$$E_e(x_e) = E_{min} + x_e^p(E_0 - E_{min}) \tag{2}$$

where E_{min} is the minimum elemental material stiffness which is set to a small value to avoid singularity and allow the load-transfer; E_0 is the initial elemental material stiffness; p is the penalization factor which, if larger than 1, will penalize the material stiffness of elements with intermediate densities. p is usually increased gradually as iterations progress, to stabilize convergence.

2.2. Sensitivity analysis

During the optimisation process, the design variables are allowed to vary continuously between 0 and 1, therefore, a gradient-based method can be used to update the design variables. The optimality criteria (OC) method has been implemented in continuum topology optimisation problem (Sigmund [8]) and has shown stable convergence efficiency, therefore, it is adopted here as the optimizer.

As shown in *Eq.* (1), the pseudo physical density x_e is the design variable. The sensitivities of the objective function (structural compliance) and constraint function (material volume) with respect to the design variable x_e can be calculated from *Eqs.* (3) and (4), respectively:

$$\frac{\partial C}{\partial x_e} = -p(E_0 - E_{min})x_e^{p-1}u_e^{\mathrm{T}}k_e u_e \tag{3}$$

$$\frac{\partial V}{\partial x_e} = A_e l_e \tag{4}$$

2.3. Optimisation procedure

During the optimisation process, at the beginning of every iteration, x_e is substituted into *Eq.* (2) to calculate the elemental material stiffness and *Eq.* (1) to calculate the structural compliance and material volume. Then, sensitivity analysis of the objective and constraint functions is carried out based on *Eqs.* (3) and (4). Based on the sensitivity information, design variables are updated using OC method. Further iterations are then carried out based on the updated design variables until the convergence criterion is satisfied. The overall optimisation procedure is detailed below as pseudocode:

1. Initialize design variable $X=1$, α, *iter* = 0, *change* = 0.1, $p = 1$ and $p_{max}=10$;
2. while *change* > 0.01 and *iter* ≤ 1000
3.   *iter* = *iter* + 1;
4.   Solve FE problem based on the design variables *X*;
5.   Calculate the objective and constraint functions, as well as their sensitivities (*Eqs.* (3 & 4));
6.   Update design variable to get X_{new} using OC method;
7.   Calculate *change* = $\| X_{new} - X \|$; $X = X_{new}$;
8.   if {*iter* > 40 and $p < p_{max}$} then p = min{(*iter*)/40, p_{max}};
9. end while.
10. Output the topology defined by the design variables *X*.

3. Benchmark examples

In this paper, a spherical gridshell structure (shown in Figure 1a) with a span of 100 m and a height of 30 m is chosen as the design example. The structure has pin-supports on all the lower nodes and members are modelled using beam elements with a uniform steel tubular section with outer diameter of 500 mm and a wall thickness of 20 mm. The steel has an elastic modulus of $E_0 = 2 \times 10^{11}$ Pa ($E_{min} = E_0/10^9$). The shell is divided into 48 elements around the base and 12 elements over a meridian, as shown in Figure 1a. The elements are grouped according to the structure's symmetry, giving 30 groups of elements that have identical structural responses under symmetric load, as depicted in Figure 1b. During the optimisation process, the densities of the independent elements are treated as design variables (and are set to 1 initially), and then adjusted each iteration until convergence. Live load acting on the roof panels in the gravity direction with a magnitude of 1 kN/m² is considered. The load is transferred to the

structure as a concentrated nodal force based on the node's tributary area. The material volume fraction α is set to 0.4.

To investigate the feasibility and efficiency of the proposed method, the structure is optimized without penalization ($p \equiv 1$) in the first example. In the second example, the penalization factor p is gradually increased to the maximum value ($p_{max}=10$) to drive the intermediate physical densities towards 0 or 1. The results of these two examples are presented in Figures 2 and 3, respectively, where Figures 2(a) & 3(a) present the optimal structures with the line thickness representing the element densities and 2(b) & 3(b) plot the associated changes of structural strain energy as iterations progress. Figures 2(c) & 3(c) report the history of the design variables during the optimisation process and 2(d) & 3(d) show the results of the KKT (Karush-Kuhn-Tucker) check in the OC process. According to the KKT conditions (Boyd and Vandenberghe [10]), at the local minimal, the differential of the Lagrangian function should be zero as a necessary condition. Therefore, the KKT condition can be applied to verify whether a true local minimum is obtained, and it is simplified herein as: $(\partial C / \partial x_e)/(\partial V / \partial x_e)$ equals to a constant for $x_e \in (0, 1)$.

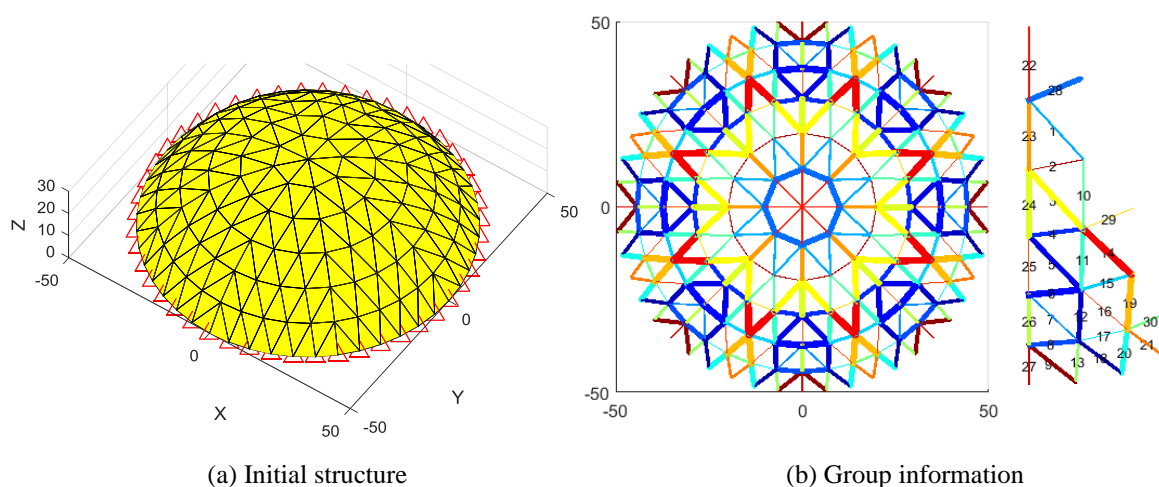(a) Initial structure   (b) Group information

Figure 1: Structural information of a spherical gridshell

3.1. Example without penalization

In Figure 2a, the elements with design variables (pseudo physical density, x_e) larger than 0.001 are shown in dark, while those with x_e less than 0.001 are in red. Without penalization, the obtained optimal structure presents a wide range of design variables and there is no clear way to identify which elements can be removed and which should remain. In Figure 2b, an increment of strain energy appears in the early iterations as the design variables were shrunk to satisfy the material volume constraint. From 25 iterations, the strain energy decreased, and the value became comparatively stable after approximately 100 iterations. Similar change can be also seen in Figure 2c, where it shows that the design variables changed significantly during the first 100 interactions and become stable afterwards. However, after optimisation, almost all the elements ended up with intermediate design variables, only Group 27 have a density close to 1, and only Groups 8, 9, 17 and 30 have densities close to zero. This is clarified in Figure 2d, the bar graph shows the ranges of the design variable and the red and green bars show the groups with the desired extreme values.

Figure 2d also shows the values of $(\partial C / \partial x_e)/(\partial V / \partial x_e)$ for each group of elements, plotted as a blue line. For elements with $0.001 < x_e < 1$, the $(\partial C / \partial x_e)/(\partial V / \partial x_e)$ values are nearly the same (marked with 'star' symbols on Figure 2d). This can be viewed as one of the evidence verifying the obtainment of a local minimum.
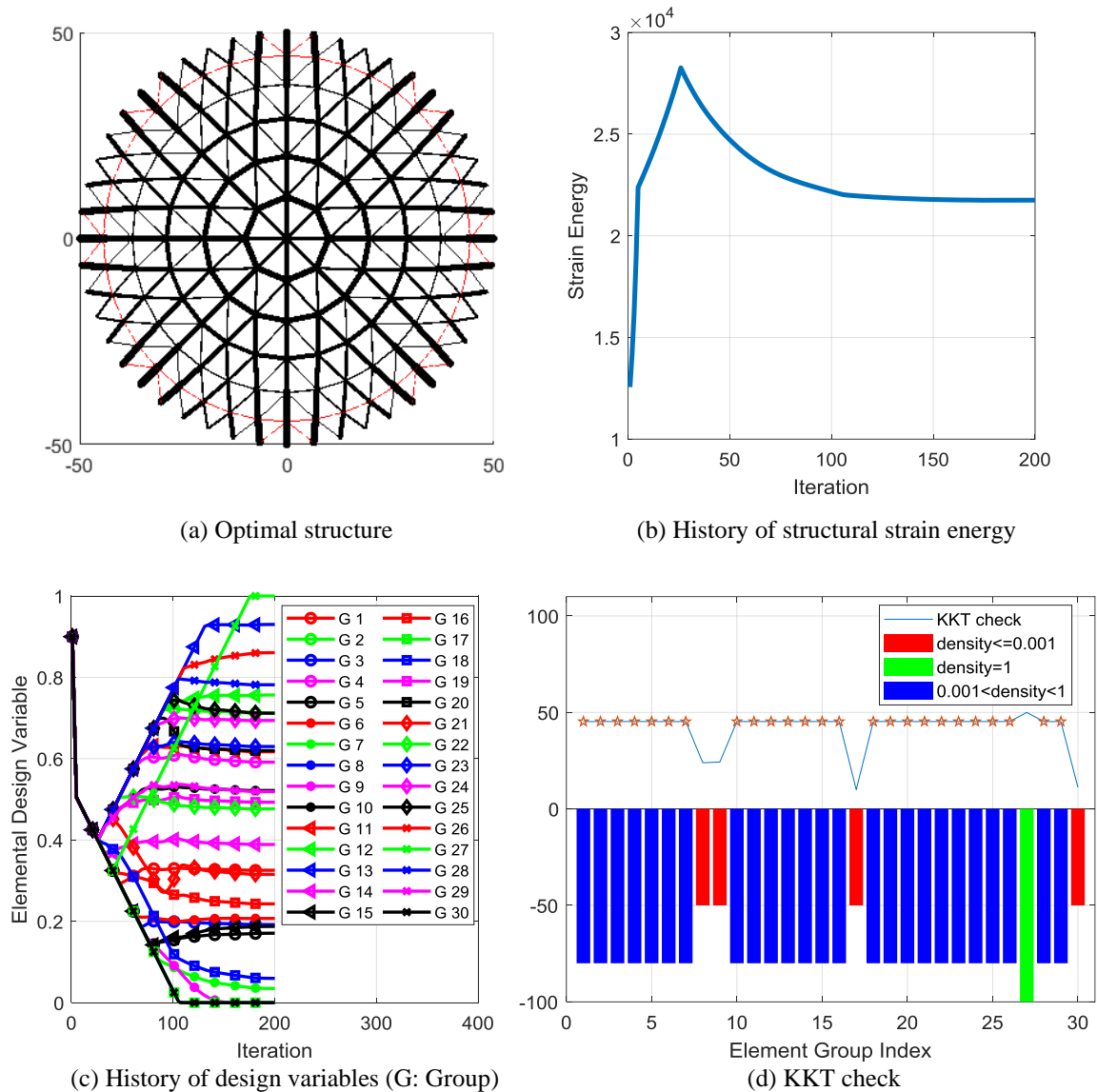
(a) Optimal structure

(b) History of structural strain energy

(c) History of design variables (G: Group)

(d) KKT check

Figure 2: Optimisation results without penalization

3.2. Example with penalization

The second example adopts exactly the same optimisation procedure as for the first, except that the penalization factor p is linearly increased from 1 to 10 between iteration 40 and 440. The resulting optimal structure is shown in Figure 3a, where it displays a clear distinction between elements that could be deleted (red lines) and those that should remain (black lines). Figure 3b shows that the structural strain energy increased until convergence, a different behaviour to the case without penalization (Figure 2b). This is partly because, with penalization, more design variables were driven towards zero. Additionally, the large penalization factor further decreases the stiffness of elements with intermediate densities, leading to the stiffness reduction of the whole structure. Figure 3c shows that the design variables changed largely at the beginning of the optimisation, and they reached a stable value after the 400th iteration, at which point the penalization factor arrived at the maximum. At convergence, 11 groups of elements were marked for deletion (as their design variables are close to 0) and the remaining elements had densities ranging between 0.6 and 0.9. In Figure 3d, the values of $(\partial C/\partial x_e)/(\partial V/\partial x_e)$ for the groups with $0.001 < x_e < 1$ were nearly the same, again verifying the obtainment of a local minimum.
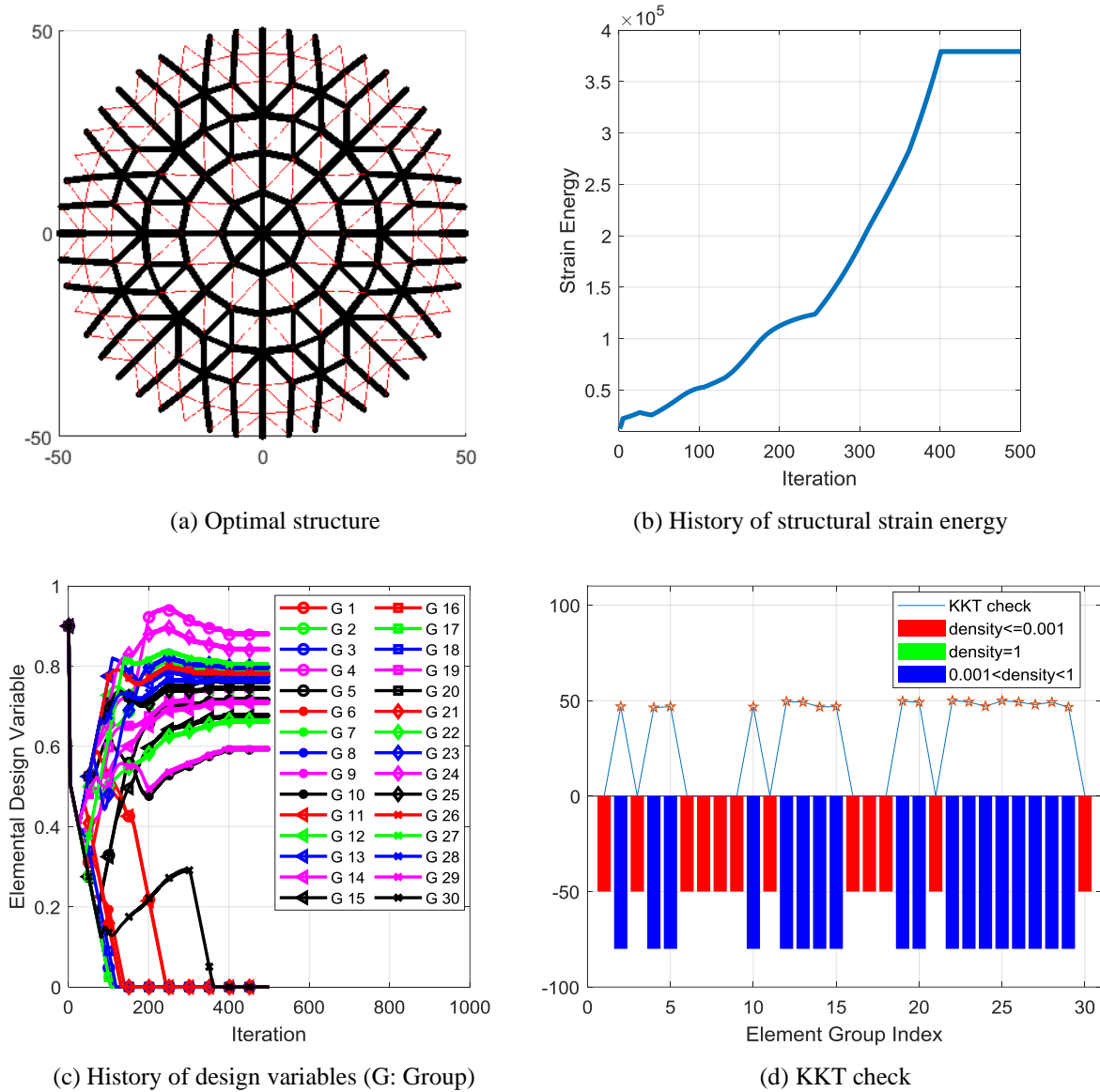
2561

(a) Optimal structure

(b) History of structural strain energy

(c) History of design variables (G: Group)

(d) KKT check

Figure 3: Optimisation results with penalization

4. Theoretical investigation on barriers to obtain binary designs

Even with penalization adopted, the algorithm still failed to guarantee a binary design (with design variables equal to purely 0 or 1), regardless of the fact that the KKT check demonstrated the achievement of a local minimum. The reasons behind this phenomenon are investigated in this section via a simple theoretical example.

A simple two-spring structure (connected in series but with different stiffnesses k_1 and k_2) is considered, as shown in Figure 4. The overall stiffness of the structure is given in *Eq.* 5:

$$k = \frac{1}{\frac{1}{k_1} + \frac{1}{k_2}} = \frac{k_1 k_2}{k_1 + k_2} \tag{5}$$

To explore why the algorithm in the examples above prefers intermediate design variables rather than binary 0 and 1 values for the optimal structure, two different combinations of design variables are assigned to the two-spring structure. The first (Combination 1) assumes the elements have distinct

design variable x_1=1 and x_2=0, the second (Combination 2) assumes intermediate design variables x_1=x_2=0.5. The structural stiffnesses corresponding to these two combinations of design variables are calculated through *Eqs*. (2) and (5) and the results are summarised in Table 1, where E_{min}=qE_0, q is a scaling factor.
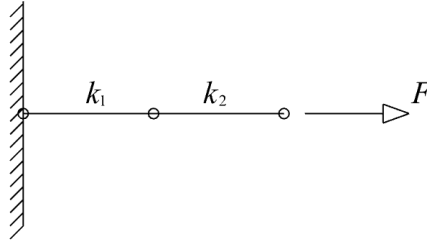

Figure 4: A two-spring structure

Table 1: The overall stiffness of a two-spring structure

	Combination 1		Combination 2	
	x_1	x_2	x_1	x_2
x	1	0	0.5	0.5
$E_e(x_e)$	E_0	E_{min}	$E_{min} + 0.5^p(E_0 - E_{min})$	$E_{min} + 0.5^p(E_0 - E_{min})$
k_{comb}	$\dfrac{E_0 E_{min}}{E_0 + E_{min}} = \dfrac{qE_0}{1+q}$		$\dfrac{qE_0 + 0.5^p E_0(1-q)}{2}$	

To guarantee a binary optimisation result, $k_{comb,1}$ must be greater than $k_{comb,2}$, therefore, the penalization factor p and the scaling factor q need to satisfy the relationship shown in *Eq*. 6 :

$$\frac{q}{1+q} > \frac{q + 0.5^p(1-q)}{2} \tag{6}$$

which gives

$$1 > 0.5^p(\frac{1}{q} + 1) \tag{7}$$

To have $k_{comb,1}$> $k_{comb,2}$, the values of p and q need to satisfy *Eq.* (7). For a series of p from 1 to 10, the corresponding minimum values of q are shown in Table 2. For example, if p=1, the minimal choice of q is 1; if p=10, q should be larger than 1/1023.

Table 2: Values of p and q satisfying *Eq.* (7)

p	1	2	3	4	5	6	7	8	9	10
q (fraction)	1	1/3	1/7	1/15	1/31	1/63	1/127	1/255	1/511	1/1023
q (decimal)	1	0.3333	0.1429	0.0667	0.0323	0.0159	0.0079	0.0039	0.0020	0.0010

As presented in Section 3, (p, q) equals to $(1, 1/10^9)$ for the first example. In the second example, p started with 1 and gradually increased up to 10, and q maintained as $1/10^9$. It is obvious that, in these two examples the values of (p, q) did not satisfy the condition set up in *Eq.* (7). Therefore, during the optimisation process, in order to result in a stiffer overall structure, adjacent elements were favoured that had intermediate design variables, rather than very large or very small design variables. Hence, the optimal structures failed to present binary included/deleted patterns of elements.

5. Extended examples

Based on the analysis in Section 4, it can be concluded that a binary optimisation result can be only achieved if suitable values of p and q are adopted in the optimisation process. For example, to obtain a binary design for the two-spring structure, if $p=10$, a q larger than $1/1023$ is needed. However, the gridshell structure is consisted of interconnected elements and is sustaining distributed load, therefore it is different from the two-spring example and the p-q relationship identified in Section 4 is not directly applicable to the gridshell. Based on the trial study done by the researcher, in general, ($p=10$, $q=1/10$) can guarantee binary optimisation results for the gridshell structure. In the following, two extended examples are provided, one with a material volume fraction α equal to 0.4 and the other equal to 0.3; both have $q = 0.1$. During the optimisation process, the penalization power p is gradually increased to 10 as before. The optimisation results are shown in Figures 4 and 5, respectively, where Figures 4a and 5a present the optimal structures and Figures 4b and 5b show the history of design variables for each group of elements.

Figure 4 shows that optimisation result to the problem with a volume fraction of 0.4, which is a purely binary design, with all the groups having elements either deleted (design variables equal to 0), or fully present (design variables equal to 1). The history of the design variables in Figure 4b reflects the fact that the penalization procedure worked successfully as the elements with higher design variables were all increased to 1 and those with smaller design variables were all penalized to zero in the optimal design, leaving no elements with intermediate design variables.

In Figure 5a, there are three more groups of elements (Groups 4, 19 and 29) marked for deletion (drawn in red) compared with Figure 4a, since the volume fraction is reduced to 0.3. Figure 5b shows that nearly all of the elements have been allocated design variables of either 0 or 1, except for Group 27. This is because the volume constraint of 0.3 cannot be achieved by including or deleting whole members, it is a constraint on volume rather than on the number of the elements included in the design.

Comparing the optimisation results provided in this section with those in Section 3.2, it can be seen that binary designs involving design variables of either 0 or 1 can be obtained if suitable values of p and q are chosen. In such cases, the optimisation results can be used to guide the second-layer grid additions in the design of partial double-layer gridshell structures.
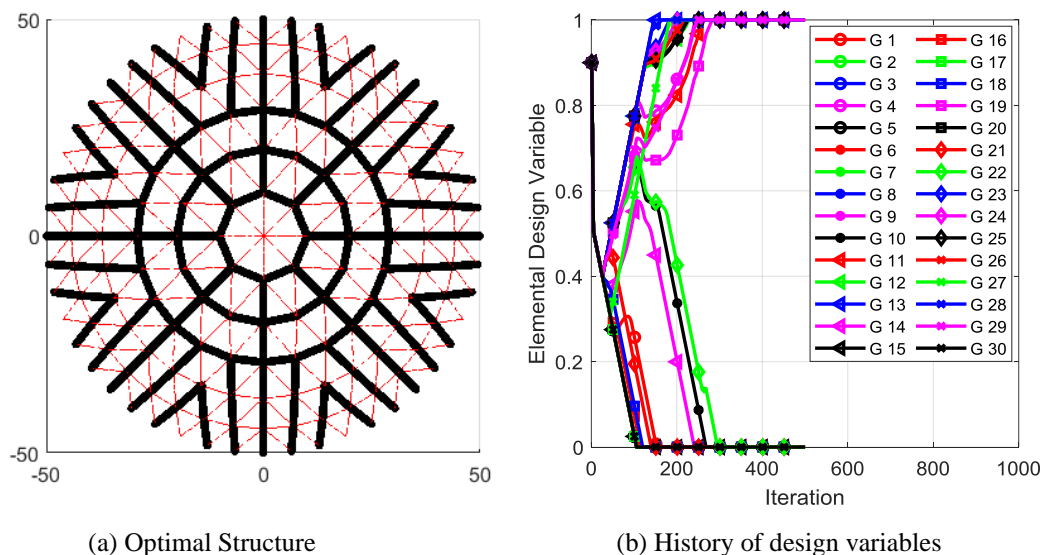

| (a) Optimal Structure | (b) History of design variables |

Figure 4: Optimisation results with volume fraction=0.4

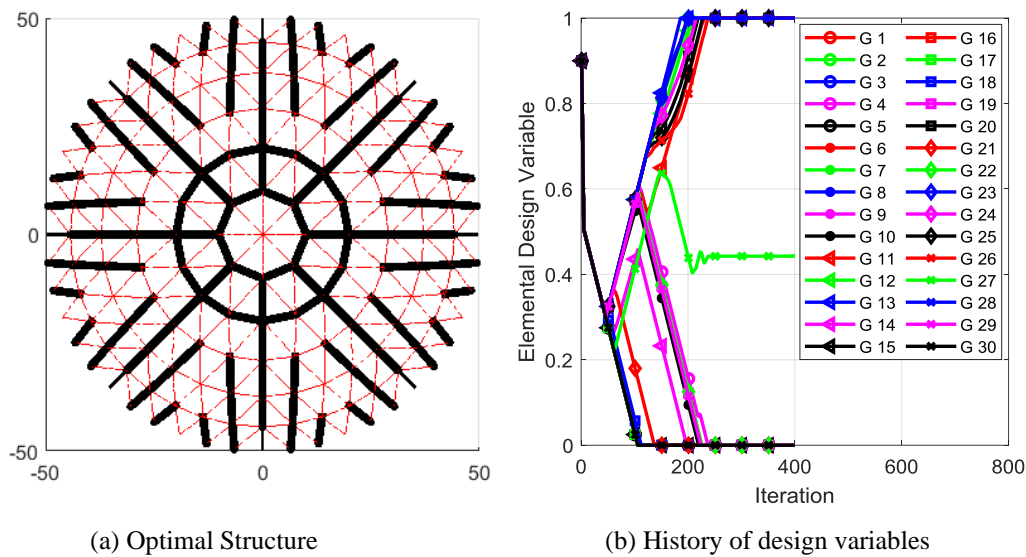(a) Optimal Structure   (b) History of design variables

Figure 5: Optimisation results with volume fraction=0.3

6. Design of a partial double-layer gridshell structure

As presented in Section 5, with a proper assignment of (p, q), binary solutions to the topology optimisation problem can be obtained. However, for the case of volume fraction=0.3, there are some isolated elements present in the optimisation result; while for the case of volume fraction=0.4, the optimal structural layout consists of smoothly connected elements. Therefore, the result corresponding to volume fraction=0.4 is adopted for the guiding paths of the second-layer grids, with the reverse V-shape paths close to the lower boundary omitted. To facilitate the addition of second-layer grids, the grid division for the gridshell structure is regenerated with the consideration of the guiding paths and the result is shown in Figure 6a, termed "Single-Shell". Based on the newly generated grids, second-layer structures are added by following the dual principle proposed by Conway *et al.* [11]. The second-layer nodes (bottom nodes) are generated by offsetting the centroids of the neighbouring faces of the guiding paths with an offset distance of 2m. Then, the bottom nodes are connected to the vertices of their affiliated faces to form web-members. The bottom chord members are generated based on the neighbouring relationship between the top faces. The obtained partial double-layer gridshell (PDouble-Shell) is shown in Figure 6b.

(a) Single-layer gridshell (Single-Shell)   (b) Partial double-layer gridshell (PDouble-Shell)
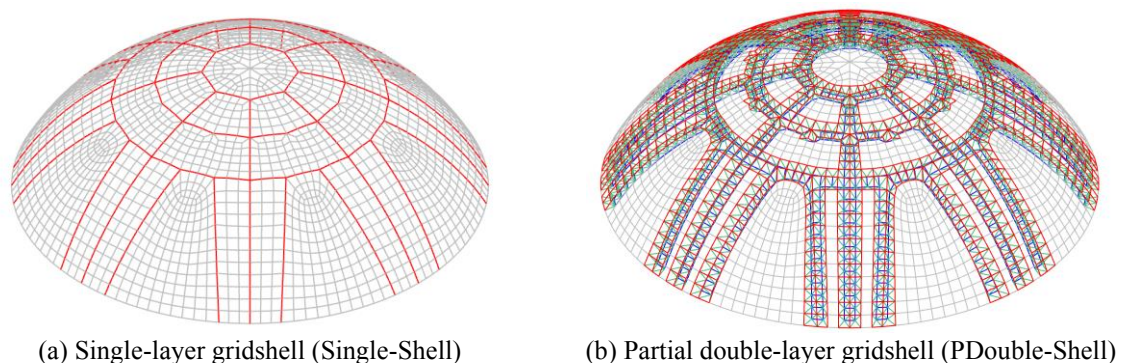
Figure 6: Sketch of the single-layer and partial double-layer gridshells

To compare the mechanical properties of the single-layer and partial double-layer gridshell, size optimisation is firstly carried out based on the fully stressed design (FSD) criteria, followed by an eigenvalue buckling analysis. Similar to the topology optimisation problem, beam elements with a

tubular section are adopted to simulate the structures. The elasticity modulus of material is 2×10^{11} Pa, the shear modulus is 7.69×10^{10} Pa and the yield stress is set as 200 MPa. Live load with an amplitude of 1kN/m^2 is applied to the top layer. The maximum stress ratio for size optimisation is set as 0.3, the optimal cross sections of structural members are shown in Table 2. The mechanical properties of the structures are presented in Table 3. The first eigenvalue buckling modes of these two structures under the external load are shown in Figure 7 with the colours representing displacement.

As shown in Table 2, the sum of the element lengths of the Single-Shell is 10285m, while it is 23709m for the PDouble-Shell, the latter being around 2.3 times the former. Nevertheless, the PDouble-Shell consumes less material compared to the Single-Shell, and this demonstrates that by properly configuring second-layer grids, the material volume of structures can be reduced. Under external load, the stress and displacement values of the PDouble-Shell are close to that of the Single-Shell, as can be seen from Table 3. The first eigenmode of the Single-Shell exhibits global buckling, while for the PDouble-Shell the buckling mainly occurs in the single-layer regions, as can be seen from Figure 7. The first eigenvalue, as well as the mean of the first ten eigenvalues, are shown in Table 3, and the values of both parameters are larger for PDouble-Shell than for Single-Shell. It can therefore be concluded that under the specified load, the strength and stiffness of the PDouble-Shell is similar to the that of the Single-Shell, as can be seen from the small difference of their stress and displacement values. However, the PDouble-Shell is more advantageous in terms of structural stability and requires less material compared to the Single-Shell. Note that since the analysis has only considered a single loading case, to demonstrate the advantages of the obtained partial double-layer gridshells over the single-layer structures under practical loading scenarios, further investigation is still required, and is ongoing by the authors.

Table 2: Size optimisation results of the single-layer and partial double-layer gridshells

	Single-Shell	PDouble-Shell		
Member	Top-layer	Top-layer	Web	Bottom-layer
Sum of member length $\sum L$ (m)	10285.29	10285.29	10185.51	3237.92
Cross section $d{\times}t$ / (mm${\times}$mm)	168.3×10.0	139.7×8.0	42.4×3.6	60.3×3.0
Material volume V /m³	51.12	40.26		

Table 3: Mechanical properties of the single-layer and partial double-layer gridshells

	Stress/MPa		Displacement/mm		Eigenvalue buckling factor	
	max	mean	max	mean	First	Mean of the first ten
Single-Shell	53.51	15.98	13.68	4.20	5.10	6.35
PDouble-Shell	55.36	15.16	9.04	4.93	7.03	8.51
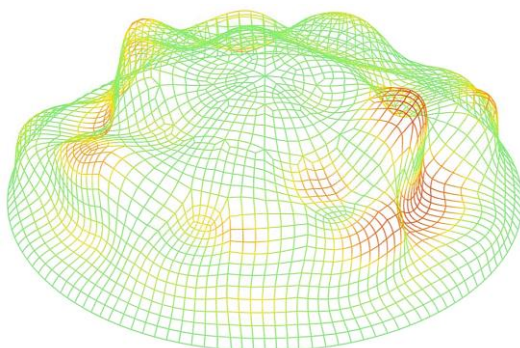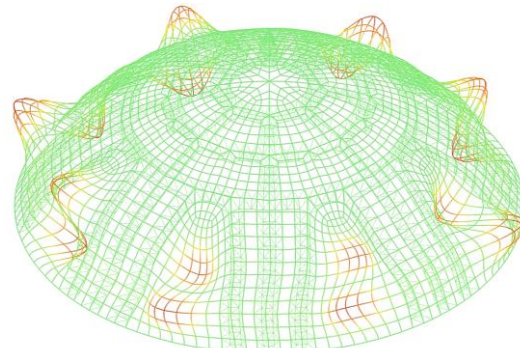
(a) Single-layer gridshell (b) Partial double-layer gridshell
Figure 7: First eigenvalue buckling mode of the single-layer and partial double-layer gridshells

7. Conclusions

In order to generate paths suitable for the addition of second-layer grids in partial double-layer gridshell structures, a topology optimisation method based on the SIMP approach has been applied to a spherical gridshell. Several benchmark examples with different combinations of optimisation parameters (E_0, E_{min} and p) are investigated, and the main conclusions drawn are as follows:

(1) When distributed load is considered, the values of the initial and minimal material stiffness of elements in the SIMP formulation should be carefully determined if a binary design without intermediate values of design variables is required.

(2) With proper assignment of the initial and minimal material stiffness, the case study demonstrates that the topology optimisation can provide binary designs, and the obtained topology suggests suitable locations for the placement of second-layer stiffening structures.

(3) By incorporating the binary topology optimisation result, a new single-layer gridshell is generated. Subsequently, a partial double-layer gridshell is formed based on the new single-layer gridshell. Mechanical analysis of the single-layer and partial double-layer gridshells demonstrate that, the partial double-layer gridshell displays similar strength and stiffness properties to the single-layer gridshell, but the former is more stable and uses less material under the specified loading compared to the latter.

Acknowledgements

References

[1] Su L., Zhu S.L., Xiao N. and Gao B.Q., An automatic grid generation approach over free-form surface for architectural design. *Journal of Central South University*, 2014; **21(6)**; 2444-2453.

[2] Li, W., Zheng, A., You, L., Yang, X., Zhang, J., & Liu, L., Rib-reinforced Shell Structure, *in Computer Graphics Forum 2014*. 2014; **36(7)**; 15-27.

[3] Tam, K. M. M., and Mueller, C. T., Stress line generation for structurally performative architectural design, *in 35th Annual Conference of the Association for Computer Aided Design in Architecture (ACADIA): Computational ecologies: design in the Anthropocene 2015*. 2015, 94-109.

[4] Michalatos, P., and Kaijima, S., Eigenshells: Structural patterns on modal forms. In *Shell Structures for Architecture* (209-224). Routledge, 2014.

[5] Wang, D., Abdalla, M. M., and Zhang, W., Buckling optimization design of curved stiffeners for grid-stiffened composite structures. *Composite Structures*, 2017; **159**; 656-666.

[6] Ji, J., Ding, X., & Xiong, M., Optimal stiffener layout of plate/shell structures by bionic growth method. *Computers & Structures*, 2014; **135**; 88-99.

[7] Lam, Y. C., & Santhikumar, S., Automated rib location and optimization for plate structures. *Structural and multidisciplinary optimization*, 2003; **25(1)**; 35-45.

[8] Sigmund, O., A 99 line topology optimization code written in Matlab. *Structural and multidisciplinary optimization*, 2001; 21(2); 120-127.

[9] Sigmund, O., Morphology-based black and white filters for topology optimization. *Structural and Multidisciplinary Optimization*, 2007; **33(4-5)**; 401-424.

[10] Boyd, S. and Vandenberghe, L., Convex optimization. *Cambridge university press*, 2004.

[11] Conway, J.H., Burgiel, H. and Goodman-Strauss, C. The symmetries of things. *CRC Press*, 2016.